Extreme Mechanics Letters 77 (2025) 102344

Contents lists available at ScienceDirect

Extreme Mechanics Letters

journal homepage: www.elsevier.com/locate/eml

Force-biased chemical degradation in rubbery networks: Insights from discrete network simulations

Lucas Mangas Araujo, Laurence Brassart *

Department of Engineering Science, University of Oxford, Oxford OX1 3PJ, United Kingdom

ARTICLE INFO

Keywords:
Rubber elasticity
Damage
Mechanochemistry
Kinetic Monte Carlo
Hydrogel
Mechanophore

ABSTRACT

This study investigates the effect of force-assisted chemical reaction leading to chain scission on the mechanical and swelling behaviour of rubbery networks. A Discrete Network (DN) modelling approach is adopted, in which polymer chains are represented as entropic springs connected at crosslink points. Force-accelerated chain scission is simulated using a Kinetic Monte Carlo algorithm. The model further accounts for degradation-induced swelling due to solvent uptake and mass loss due to the release of chain clusters detached from the main network. Discrete Network simulations highlight the role of force heterogeneities on the degradation of mechanical properties. Chains bearing the largest forces are cut preferentially, which accelerates the reduction in modulus and loss of percolation. When degradation occurs under constraint, force-biased degradation leads to anisotropic residual elastic properties. These effects cannot be captured by a state-of-the-art micromechanics-based continuum model, which does not account for the redistribution of forces through the network. Overall, the discrete network framework provides a promising platform to study a broader range of mechano-chemical phenomena in elastomers and gels.

1. Introduction

Rubbery networks are susceptible to chemical degradation when exposed to environmental factors, such as moisture, oxygen, heat, or light [1,2]. Chemical degradation often involves the breaking of load-bearing polymer chains, leading to a reduction in mechanical properties such as elasticity, strength and toughness. Conversely, chemical degradation in rubbery networks can be accelerated by mechanical forces. Under an applied force, the potential energy landscape of reactive bonds along the polymer chain shifts, facilitating chain scission by bond rupture [3]. Previous experimental works suggest that force-biased chain scission determines the strength of polymers degrading under load [4,5], and could be responsible for environmental cracking of elastomers [6,7]. Force-assisted chemical reactions are also exploited by incorporating mechanophores into rubbery networks to achieve various mechano-responsive effects, such as toughening, self-growth, or directed degradation [8–10]. In these scenarios, the evolving structure of the network plays a key role, as it governs the partitioning of forces among the chains.

In recent years, Discrete Network (DN) computational models have emerged as promising tools to investigate structure–property relationships in rubbery networks [11–15]. In this approach, the rubbery network is represented as a network of nonlinear springs with force–extension relationship derived from statistical mechanics considerations. The distribution of forces among the chains is determined from the condition of force balance at the crosslinks. Compared to semi-analytical micromechanical models of rubber elasticity, such as the eight-chain or full-network models [16,17], their main advantage is that they explicitly account for the network topology and do not require ad-hoc assumptions regarding the partitioning of the chain stretches. They are also much more cost-effective than (coarse-grained) molecular dynamics simulations. DN models have been used to investigate the role of network defects and heterogeneities on the properties of rubbery networks [12,14,15,18,19], as well as their damage and fracture mechanisms [13,20–23]. However, DN models of elastomers and hydrogels have rarely been exploited in the context of mechanically-activated chemical reaction.

In this work, we combine a DN model with a stochastic chain scission algorithm to investigate force-biased chemical degradation in rubbery networks. For the sake of generality, we consider swollen networks (e.g. hydrogels), where degradation is accompanied by swelling and mass loss, which are also accounted for in our modelling framework. Examples of applications include biodegradable hydrogels for biomedical applications such as bioresorbable implants, drug delivery

* Corresponding author.
E-mail address: laurence.brassart@eng.ox.ac.uk (L. Brassart).

https://doi.org/10.1016/j.eml.2025.102344
Received 28 November 2024; Received in revised form 14 April 2025; Accepted 23 April 2025
Available online 8 May 2025

and tissue engineering [24–26], where precise control of the degradation and mechanical properties is critically needed. Recent experimental evidence suggests that the swelling of cross-linked networks can generate chain forces that are sufficient to assist bond cleavage reactions [27–29].

We use our DN model to elucidate the role of force-biased degradation kinetics on the evolution of mechanical and swelling properties. We show that force-biased reaction kinetics accelerates degradation (as expected), and further that it amplifies the reduction in elastic modulus for a given number of chain scission events, due to preferential scission of highly-stretched chains. We also show that force-biased reaction kinetics induces anisotropic damage when degradation occurs under constraint. These trends cannot be captured by a simple continuum model based on the commonly-used eight-chain assumption, where all chains carry the same force. Overall, our work demonstrates the potential of DN models to simulate coupled chemo-mechanical phenomena in rubbery networks, and highlights the role of heterogeneous force distribution in the evolving network on the mechanical and degradation behaviour.

2. Discrete network model

2.1. Thermodynamics

We consider a network of long polymer chains held together by chemical (non-degradable) crosslinks. In the reference configuration, taken as the initial, undegraded configuration, the network is stress-free and the water concentration is C_0. The use of a pre-swollen state as reference state is convenient to describe hydrogels prepared in solution. In the DN modelling framework, polymer chains are represented as entropic springs connected at nodes representing the crosslinks. A representative DN structure is shown in Fig. 1. At any degradation stage, the free energy associated with stretching the polymer chains in the network is given by:

$$\psi^e = \frac{1}{V_0}\sum_{j=1}^{n} w^{(j)}, \tag{1}$$

where V_0 is the volume of the network in the reference configuration, $w^{(k)}$ is the free energy of the jth chain and n is the current number of chains in the network. The chain behaviour is described by the freely-jointed chain model:

$$w = Nk_BT\left[\frac{r\beta}{Nb} + \log\left(\frac{\beta}{\sinh\beta}\right)\right], \quad \beta = \mathcal{L}^{-1}\left(\frac{r}{Nb}\right), \tag{2}$$

where b is the Kuhn length, N is the number of Kuhn segments, k_B is the Boltzmann constant, T is the absolute temperature, and r is the chain end-to-end distance. The Langevin function $\mathcal{L}(x)$ is defined as $\mathcal{L}(x) = \coth(x) - 1/x$. The force needed to maintain a given end-to-end distance r is derived from the free energy as $f = \frac{dw}{dr}$:

$$f = \frac{k_BT}{b}\mathcal{L}^{-1}\left(\frac{r}{Nb}\right). \tag{3}$$

The end-to-end distance of a chain in the reference configuration is denoted as r_0. For small chain extension $r \ll Nb$, the force–extension relation (3) reduces to the Gaussian chain model:

$$f = 3k_BT\frac{r}{Nb^2}. \tag{4}$$

The Gaussian chain approximation holds for $r \lesssim 0.3Nb$. In this work, we limit ourselves to monodisperse networks where the number of Kuhn segments is the same in each (undegraded) chain.

We also endow the network with a mixing free energy to describe swelling by absorption of water. Let C be the nominal concentration of water (number of water molecules per unit volume in the reference state) and ϕ be the current volume fraction of polymer. The free energy contribution due to mixing the water molecules with the long polymer chains is given by the Flory–Huggins model [30,31]:

$$\psi^c = \mu_0 C + \frac{k_BT}{\Omega}J\left[(1-\phi)\log(1-\phi) + \chi\phi(1-\phi)\right], \tag{5}$$

where μ_0 is a reference chemical potential for water, Ω is the volume per water molecule, χ is the affinity parameter, and $J \equiv \det(\boldsymbol{F})$ is the swelling ratio with respect to the reference configuration. Note that water molecules are not represented explicitly in the DN framework. The total free energy of the swollen network is given by $\psi = \psi^e + \psi^c$.

Coupling between rubber elasticity and absorption of water is achieved by assuming molecular incompressibility. The swelling ratio J (ratio of current volume to the volume in the reference configuration) is then directly related to the current amount of polymer and water by Pan and Brassart [32]:

$$J = 1 - m\phi_0 + \Omega(C - C_0), \tag{6}$$

where ϕ_0 represents the polymer volume fraction in the reference configuration. $m \equiv \frac{V_{p0}-V_p}{V_{p0}}$ is the polymer mass loss fraction, with V_{p0} and V_p the reference and current volumes of polymer (the density of polymer is assumed constant). Thus, Eq. (6) accounts for the change in volume due to releasing polymer chains during degradation, in addition to the change in volume due to absorption of water. In the initial, reference state, $C = C_0$, $m = 0$ and $J = 1$, as required. Also note the following relation between the polymer volume fraction and the water concentration: $(1-\phi) = \frac{\Omega C}{J}$. In the reference state, $J = 1$ and $(1-\phi_0) = \Omega C_0$.

The network is subjected to a prescribed deformation gradient $\boldsymbol{F}$, with $J = \det(\boldsymbol{F})$. The reference configuration is defined such that $\boldsymbol{F} = \boldsymbol{1}$ and $C = C_0$. In the current configuration, the network is subjected to a macroscopic stress $\boldsymbol{P}$ and is in contact with a reservoir of water with chemical potential μ. We assume that the network is always at equilibrium with respect to the applied stress and chemical potential:

$$\boldsymbol{P} : \delta\boldsymbol{F} + \mu\delta C + \Pi(\delta J - \Omega\delta C) - \delta\psi = 0, \tag{7}$$

where Π represents a Lagrange multiplier enforcing the kinematic constraint (6). In writing Eq. (7), we consider virtual deformation and concentration changes $(\delta\boldsymbol{F}, \delta C)$ with no chain degradation or mass loss. Eq. (7) means that we do not account for viscoelasticity, and that we assume chemical equilibrium. This assumption holds considering that water diffusion is much faster than chemical degradation. Noting the result $\delta J = J\boldsymbol{F}^{-T} : \delta\boldsymbol{F}$, the state laws for the stress and chemical potential are obtained:

$$\boldsymbol{P} = \frac{\partial\psi^e}{\partial\boldsymbol{F}} - J\Pi\boldsymbol{F}^{-T}, \tag{8}$$

$$\mu = \frac{\partial\psi^c}{\partial C} + \Omega\Pi. \tag{9}$$

The Cauchy stress is obtained from the classical relation $\boldsymbol{\sigma} = (1/J)\boldsymbol{P}\boldsymbol{F}^T$.

The macroscopic deformation $\boldsymbol{F}$ is applied by prescribing the displacement of the n_b boundary nodes of the network according to the affine relation:

$$\boldsymbol{x}_\alpha = \boldsymbol{F}\boldsymbol{X}_\alpha, \quad \alpha = (1, n_b), \tag{10}$$

where $\boldsymbol{X}_\alpha$ and $\boldsymbol{x}_\alpha$ respectively represent the coordinates of the αth boundary node in the reference and current configurations. Consistent with Eq. (7), the network is assumed to be at equilibrium at all times, i.e. force balance is satisfied at each node. The network stress contribution can then be obtained as Alamé and Brassart [19]:

$$\boldsymbol{P}^e \equiv \frac{\partial\psi^e}{\partial\boldsymbol{F}} = \frac{1}{V_0}\sum_{\alpha=1}^{n_b}\boldsymbol{f}^r_\alpha \otimes \boldsymbol{X}_\alpha, \tag{11}$$

where $\boldsymbol{f}^r_\alpha$ is the reaction force on boundary node α. The corresponding Cauchy stress is given by $\boldsymbol{\sigma}^e = (1/J)\boldsymbol{P}^e\boldsymbol{F}^T$. Note that the network stress $\boldsymbol{P}^e$ does not vanish in the reference configuration. According to the force extension relation (3), a non-zero initial chain end-to-end distance

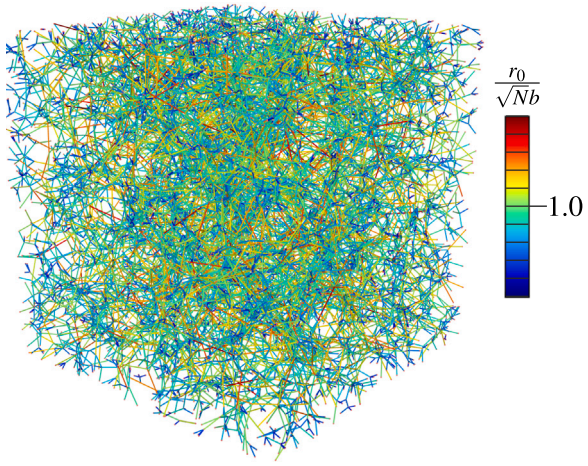

Fig. 1. Representative discrete network with $n = 20000$ chains in the equilibrated reference configuration, showing the initially-heterogeneous distribution of chain end-to-end distances.

r_0 requires a non-zero chain force, leading to a non-zero macroscopic stress $\boldsymbol{P}^e$ according to Eq. (11). A representative initial distribution of r_0 in the equilibrated reference configuration is shown in Fig. 1. Using the Flory–Huggins model (5), the state law for the chemical potential (9) can be re-expressed as:

$$\mu = \mu_0 + k_B T \left[\log(1-\phi) + \phi + \chi\phi^2\right] + \Pi\Omega. \tag{12}$$

The Lagrange multiplier Π is determined from the boundary conditions.

2.2. Degradation: Kinetic Monte Carlo algorithm

The kinetics of chain scission by chemical reaction of susceptible backbone bonds is described using an Eyring-type model [33,34]:

$$k = \gamma \exp\left(-\frac{U_b - f a}{k_B T}\right) = k_0 \exp\left(\frac{f a}{k_B T}\right), \tag{13}$$

where γ is the attempt frequency, U_b is the activation energy for bond scission by chemical reaction in the absence of an applied force, and a is an activation length. $k_0 \equiv \gamma \exp\left(-U_b/k_B T\right)$ represents the scission rate in the absence of an applied force. In this work, we assume that each chain contains at most one reactive bond, so that Eq. (13) directly provides the chain scission rate under a given applied force. For chains that do not contain any reactive bond, the rate constant k_0 is simply set to zero. Given a population of n identical chains subjected to a constant force, the number of surviving chains is described by a first-order kinetic model: $\dot{n} = -kn$, and the survival probability of a chain after time t is given by: $p_s(t) = \exp(-kt)$.

In writing Eq. (13), we have implicitly identified the chain force f with the bond force, which is a strong approximation. In a real polymer chain, the bond force becomes significant only when the chain is highly extended under large force, whereas it is negligible when the chain stretch is small. In this work, we used the (purely entropic) freely-jointed chain model to describe the force–extension response of a single chain for simplicity. Since this model does not provide an estimate of the bond force, the chain force was used in Eq. (13). Within the DN framework, the distinction between bond force and chain force could be captured by adopting a single-chain model that accounts for energetic effects to the chain behaviour, such as the extendable freely-jointed chain model (which accounts for stretchable bonds) [35] or the deformable freely-rotating chain model (which accounts for both bond stretching and bond angle opening) [36]. This extension of the DN framework will be considered in a future work.

In the DN, the distribution of forces among the chains is non-homogeneous, giving a distribution of chain scission rates $k^{(j)}$. Any chain scission event corresponds to a change of state of the network as a whole. The rate of escape of the network from its current state is given by:

$$k_{tot} = \sum_{j=1}^{n} k^{(j)}. \tag{14}$$

The rate k_{tot} represents the total escape rate in a population of identical networks. The survival probability of the network in its current state is given by: $P_s(t) = \exp(-k_{tot}t)$, i.e. $P_s(t)$ is the probability that no chain scission occurs in the network within at time interval t. Equivalently, $(1 - P_s(t))$ is the probability that (at least) one chain scission occurs within the same time t. By definition of the cumulative distribution function, the probability distribution of the time of first chain scission event $P(t)$ is obtained by integrating the function $(1 - P_s(t))$ [37]:

$$P(t) = k_{tot} \exp(-k_{tot}t). \tag{15}$$

In the Kinetic Monte Carlo (KMC) algorithm, the degradation process is simulated by cutting one chain every time interval Δt, where Δt is drawn from the probability distribution of the time of first chain scission (15). In practice, this is readily achieved by drawing a uniformly distributed random number $\xi_1 \in]0, 1]$, and using the following formula [37]:

$$\Delta t = -\frac{1}{k_{tot}} \log(\xi_1), \tag{16}$$

which is obtained by inverting the cumulative distribution function $(1-P_s)$, also using the fact that ξ_1 and $1-\xi_1$ follow the same distribution. The chain j to be broken is randomly selected, such that it satisfies the following criterion:

$$\sum_{1}^{j-1} k^{(j)} < \xi_2 k_{tot} < \sum_{1}^{j} k^{(j)}, \tag{17}$$

where $\xi_2 \in [0, 1]$ is a second uniformly distributed random number. In the case where the chain force has no effect on the chain scission rate ($k^{(j)} = k_0$), all the chains are equally likely to be broken according to the selection criterion (17). However, when reaction is accelerated by the chain force, the criterion (17) favours the scission of chains experiencing large forces.

2.3. Mass loss

We assume that mass loss occurs due to the formation of elastically-ineffective chains, or chain clusters, and which are detached from the main network due to chain scission. Chain clusters are identified with the connected components of the network, treated as a graph. Two connected components of the network (graph) are such that there is no chain (edge) connecting their respective nodes. Chain clusters are removed from the network if the following two conditions are met: (1) all the chains in the cluster are elastically ineffective (i.e. they bear zero force), and (2) the number of chains in the cluster is less than a threshold value n_d. The second condition physically corresponds to the requirement that chain clusters should be small in comparison to the mesh size to be able to diffuse out of the network. Note that we assume that diffusion of the clusters is much faster than degradation, and therefore we do not account for diffusion kinetics.

After removal of a chain cluster, the number of remaining chains n in the network is recalculated. We also count the number n_1 of complete chains with N Kuhn segments, and the number n_2 of dangling chains with $\frac{N}{2}$ Kuhn segments, so that $n = n_1 + n_2$. The mass loss m is then calculated as:

$$m = 1 - \frac{\left(n_1 + \frac{n_2}{2}\right)}{\left(n_{1,0} + \frac{n_{2,0}}{2}\right)}, \tag{18}$$

where $n_0 = n_{1,0} + n_{2,0}$ is the initial number of chains. Eq. (18) accounts for the fact that dangling chains contribute half the mass of a complete chain.

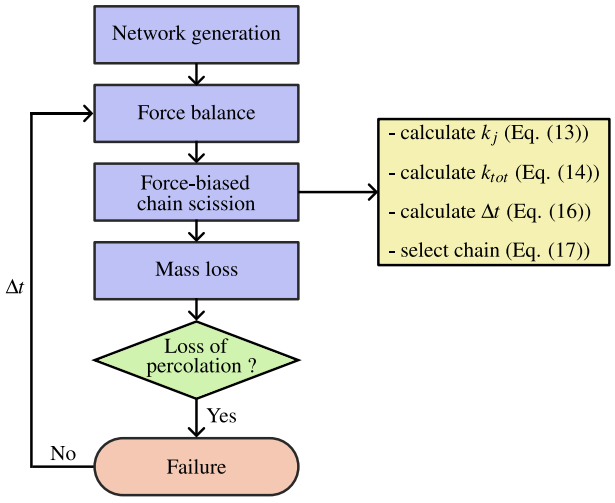

Fig. 2. Numerical procedure for coupled mechanics and degradation of discrete networks using a Kinetic Monte Carlo algorithm.

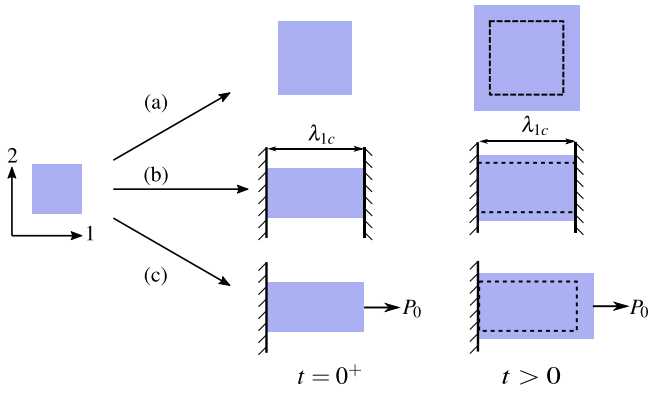

Fig. 3. Degradation scenarios considered in this work: (a) free degradation, (b) degradation under a constant pre-stretch λ_{1c}, and (c) degradation under a dead load P_0. Diffusion of water and detached chain clusters is assumed much faster than degradation.

2.4. Numerical procedure

Discrete networks were generated in cubic simulation volumes using our in-house algorithm implemented in Matlab, which allows control of chain density and end-to-end distance distribution independently by allowing chains to interpenetrate, see Araujo et al. [15] for details. All the crosslinks have a coordination of four, and we do not consider second-order loops. Discrete networks had at least 20000 chains in their initial undegraded state, which is sufficiently large to ensure that the networks are statistically representative and isotropic.

Networks were subjected to macroscopic deformation gradients $\boldsymbol{F} = \{\lambda_1, \lambda_2, \lambda_3\}$, where λ_i $(i = 1, 2, 3)$ are the principal stretches along the cube faces, following Eq. (10). At every time step, networks were equilibrated using LAMMPS [38] and the chain forces were calculated. Network structures were then updated to account for chain scission and mass loss, following the procedure outlined in Sections 2.2 and 2.3. We assume that the network fails at the percolation threshold, also called reverse gelation point, identified here as the time where there is no continuous chain path connecting any pair of opposing faces in the simulation volume. At this point, the simulation stops. The stochastic degradation model was implemented in `Python` using the `networkx` library for graph-related operations. In practice, to reduce the computational cost, mass loss calculation, loss of percolation detection and network re-equilibration were carried out every 60 chain scission events. We have verified that this simplification has negligible impact on the numerical results. The numerical steps are illustrated in Fig. 2. The different degradation scenarios considered in this work are illustrated in Fig. 3, and details of the boundary conditions are provided in Appendix A.1. As an illustration, the DN model is used to simulate degradation-induced swelling in tetra-PEG hydrogels in Appendix B, where numerical predictions are also compared to the experimental data of [39].

2.5. Degraded elastic modulus

We characterise the effect of chemical degradation on the mechanical properties by calculating the elastic modulus of the network in the undegraded and degraded states. For uniaxial deformation along direction 1 at constant water content, $\lambda_2 = \lambda_3 = 1/\sqrt{\lambda_1}$, and the Young modulus can be calculated as:

$$E_0 = \lim_{\lambda_1 \to 1} \frac{d\sigma_1}{d\lambda_1}, \tag{19}$$

where σ_1 is the principal Cauchy stress in direction 1. For an incompressible, isotropic elastic material, the shear modulus is related to the Young modulus by $E_0 = 3G_0$. In the particular case where all the network chains are in their Gaussian regime in the reference configuration, i.e. $r_0 \lesssim 0.3Nb$, the shear modulus can alternatively be calculated as Alamé and Brassart [19]:

$$G_0 = \nu_0 k_B T \left\langle \frac{r_0^2}{Nb^2} \right\rangle, \tag{20}$$

where ν_0 is the number density of elastically-effective chains in the undegraded network (number of chains per unit volume in the reference configuration). The notation $\langle\cdot\rangle$ denotes the average over all the chains in the network. Eq. (20) is exact provided that the network is isotropic. The validity of formula (20) has been verified in our previous work [15]. Eq. (20) recovers the classical expression $G = \nu_0 k_B T$ only in the specific case where the root-mean-square average of the chain end-to-end distance is equal to the random walk distance $\sqrt{N}b$.

We define the elastic moduli of the degraded network w.r.t. to a fictitious "damaged reference configuration", which is obtained by bringing the degraded network to a state with $\boldsymbol{F} = \boldsymbol{1}$. The incompressibility condition (6) for $J = 1$ and the current mass loss fraction m together dictate the value of C in the degraded configuration. The degraded Young modulus in direction i can be obtained by subjecting the degraded network to a uniaxial tension test in direction i:

$$E_i = \lim_{\tilde{\lambda}_i \to 1} \frac{d\sigma_i}{d\tilde{\lambda}_i}, \tag{21}$$

where $\tilde{\lambda}_i$ is the principal stretch in direction i measured w.r.t. the damaged reference configuration. As shown later, force-induced degradation can result in anisotropic elastic properties in the damaged state, so that the three degraded Young moduli may differ. In the particular case where the network remains isotropic in the degraded state, $E_1 = E_2 = E_3 \equiv 3G$. Further assuming Gaussian chain behaviour, the degraded shear modulus G can be obtained as:

$$G = \nu k_B T \left\langle \frac{\tilde{r}_0^2}{Nb^2} \right\rangle, \tag{22}$$

where ν is the current density of elastically-effective chains (number of chains per unit volume in the reference configuration), and $\tilde{r}_0$ is the end-to-end distance of a chain in the damaged reference configuration. In general, $\tilde{r}_0 \neq r_0$ for a given chain, because the topology of the degraded network differs from that of the undegraded network, impacting the partitioning of stretches among the chains and hence the modulus.

3. Continuum model

We also consider a simple analytical model and compare its performance against predictions of the DN model to gain better understanding

of the impact of simplifying assumptions. For simplicity, we neglect mass loss and focus on the effect of degradation on the elastic and swelling behaviour. Like in the DN model, the mixing energy is described using the Flory–Huggins model, Eq. (5). For the elastic energy of the network, we adopt the eight-chain representation [16], which is based on a simplified unit cell of the network consisting of eight identical freely-jointed chains meeting at its centre. The eight chains all experience the same stretch, so that the network free energy is simply given by:

$$\psi^e = \nu N k_B T \left[\frac{r\beta}{Nb} + \log\left(\frac{\beta}{\sinh\beta}\right)\right], \quad \beta = \mathcal{L}^{-1}\left(\frac{r}{Nb}\right). \tag{23}$$

For a degrading network, the density of elastically-effective chains ν is not constant but decreases with the extent of degradation. Consistent with the kinetic model of degradation introduced in Section 2.2, the chain density is taken to evolve following a first-order kinetic equation [40]:

$$\dot{\nu} = -\nu k_0 \exp\left(\frac{f a}{k_B T}\right), \tag{24}$$

where the chain force is related to the current chain end-to-end distance by the force–extension relation (3). The initial condition is $\nu = \nu_0$ at $t = 0$, corresponding to the undegraded reference state. We also define the ratio $\eta \equiv \frac{\nu}{\nu_0}$.

The chain end-to-end distance in the degraded network is calculated as:

$$r = \Lambda \tilde{r}_0, \tag{25}$$

where Λ is the chain stretch, which in the eight-chain representation is given by:

$$\Lambda = \sqrt{\frac{I_1}{3}}, \quad I_1 = \lambda_1^2 + \lambda_2^2 + \lambda_3^2. \tag{26}$$

In Eq. (25), $\tilde{r}_0$ is the chain end-to-end distance in the degraded reference configuration. The localisation rule (25) thus accounts for the effect of damage on the localisation of chain stretch. In the reference, undegraded state, $\tilde{r}_0 = r_0$. As the network degrades, $\tilde{r}_0$ evolves. Note that the continuum damage model is isotropic, since the effect of damage is described via scalar parameters only: the current density of elastically-effective chains ν and the chain end-to-end distance in the degraded state $\tilde{r}_0$.

The evolution of $\tilde{r}_0$ is defined based on the following considerations. First, using the localisation rule (25) into the elastic energy (23), it can be shown that the elastic shear modulus of the eight-chain model w.r.t. the reference and degraded reference states are respectively given by:

$$G_0 = \nu_0 k_B T \frac{r_0^2}{Nb^2}, \tag{27}$$

and:

$$G = \nu k_B T \frac{\tilde{r}_0^2}{Nb^2}, \tag{28}$$

which parallel Eqs (20) and (22) for an (isotropic) DN. In particular, Eqs (20) and (27) show that the shear modulus of the eight-chain model coincides with the undegraded DN modulus provided that r_0 is set to the root-mean-square average of the initial chain end-to-end distance $\sqrt{\langle r_0^2\rangle}$ in the DN. The importance of matching the initial chain end-to-end distance in DN and continuum models for meaningful comparison was highlighted in our previous works [15,19]. Taking the ratio of Eqs (27) and (28), we obtain:

$$\frac{G}{G_0} = \eta \frac{\tilde{r}_0^2}{r_0^2}. \tag{29}$$

For a network of Gaussian chains with fixed volume but decreasing number of chains, the evolution of the modulus as a function of η can be reasonably well described by the Effective Medium Approximation (EMA) [19,41,42]:

$$\frac{G}{G_0} \approx 2\eta - 1. \tag{30}$$

Using the EMA into Eq. (29), the evolution equation for the reference degraded distance is obtained:

$$\frac{\tilde{r}_0}{r_0} = \sqrt{\frac{2\eta - 1}{\eta}}. \tag{31}$$

Under the EMA, the evolution Eq. (31) ensures that the ratio G/G_0 predicted by the eight-chain model and the DN coincide by construction.

Application of the continuum model as an approximation of a given DN simulation involves the following steps. Consistent with the DN model, the reference state, taken as the initial undegraded state, corresponds to $\boldsymbol{F} = \boldsymbol{1}$ (by definition), $C = C_0$ and $\boldsymbol{P} = \boldsymbol{0}$. For a given initial chain density ν_0 (the same as in the corresponding DN model), the chain end-to-end distance r_0 is set to the root-mean-square average of the chain end-to-end distance in the DN, which ensures that the initial modulus G_0 coincides with the DN modulus. Also, $\tilde{r}_0 = r_0$ in the initial, undegraded state. For a given deformation gradient, the chain stretch is calculated according to Eq. (26), and the chain force is calculated using the freely-jointed chain model. Next, the chain density is evolved according to Eq. (24) and η is updated. The degraded end-to-end distance $\tilde{r}_0$ is updated using Eq. (31). At each degradation stage, the stress, chemical potential and Lagrange multiplier are calculated from the state laws (8)–(9) and boundary conditions. The simulation is terminated when $\eta = 0.5$, corresponding to $G = 0$ according to the EMA (30).

4. Results

We use the DN model to investigate the effect of force-assisted chemical degradation on the mechanical and swelling behaviour of rubbery networks. We also compare DN results semi-analytical estimates using the continuum model. The following scenarios were considered: (a) free degradation, (b) degradation under a constant pre-stretch, and (c) degradation under a dead load, as represented in Fig. 3. Material parameters were set as follows: $N = 29$ and $b = 1.1$ nm, and $\phi_0 = 10\%$, giving the initial water concentration as $C_0 = \frac{1-\phi_0}{\Omega}$ with $\Omega = 0.03$ nm^3. The initial chain density ν_0 was obtained from the initial volume fraction as $\nu_0 = \phi_0/v_{ch}$, where $v_{ch} = N v_m$ is the volume of a polymer chain and v_m the volume of a Kuhn monomer, set as $v_m/\Omega = 2.2$. Random discrete networks were generated so that the square average initial end-to-end distance is $\langle r_0^2\rangle \approx Nb^2$, so that $G_0 = \nu_0 k_B T$ according to Eq. (20). Finally, we set $\chi = 0.45$, $T = 310$ K and $k_0 = 16.5 \times 10^{-4}$ h^{-1}.

4.1. Free degradation

We first consider free degradation, as illustrated in Fig. 3(a). At time $t = 0^+$, the undegraded network is immersed in a water bath with chemical potential $\mu = \mu_0$ and instantaneously swells to its equilibrium value $J = J_0$. At $t > 0$, the network degrades and swells further, until it reaches the point of reverse gelation. Details of boundary conditions are given in Appendix A.1. For illustration, snapshots of a discrete network at different stages of degradation are shown in Fig. 4, where the degradation state is quantified by the normalised number of chain scissions ζ (the ratio of the number of chain scission events to the initial number of chains).

Fig. 5(a) shows the evolution of the normalised number of chain scissions ζ for different values of the activation length a and $n_d = 0$ (no mass loss). As expected from the kinetic model (13), increasing a results in accelerated degradation, noting that chains are always under tension even when the network is subjected to zero stress. The critical value ζ_c

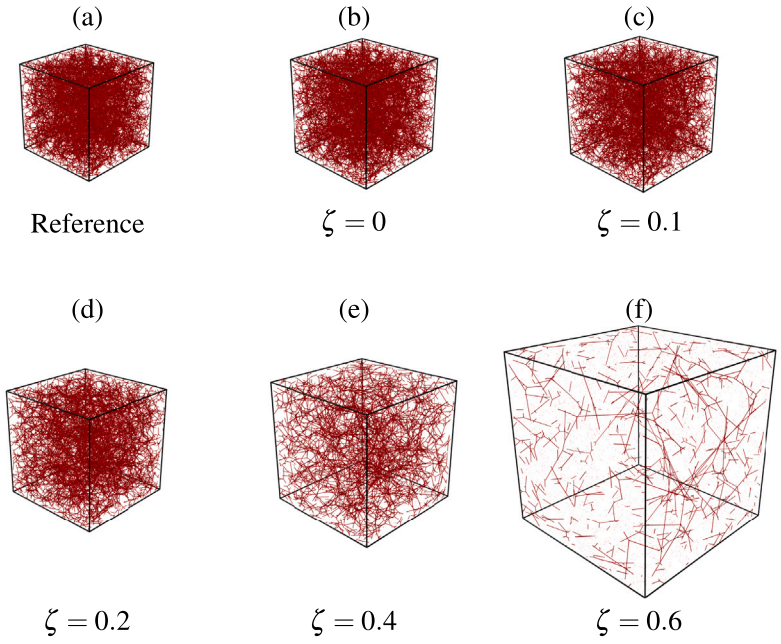

Fig. 4. Visualisation of degradation-induced swelling in the absence of applied stress for a network with $a = 0$ and $n_d = 0$. Only the non-broken chains are shown. (a) Reference configuration of the undegraded network. (b) Equilibrium free-swollen state at the onset of degradation ($\zeta = 0$). (c)–(f) Equilibrium free-swollen states at different degradation stages: (c) $\zeta = 0.1$, (d) $\zeta = 0.2$, (e) $\zeta = 0.4$ and (f) $\zeta = 0.6$. The final snapshot represents the state immediately before loss of percolation.

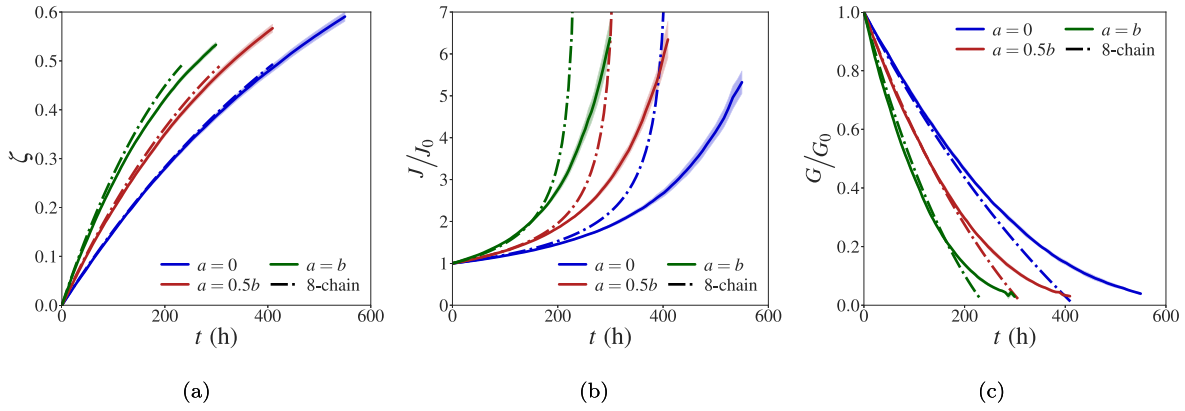

Fig. 5. (a) Normalised number of chain scissions, (b) normalised swelling ratio, and (c) normalised degraded shear modulus as a function of time. Continuous lines represent average DN predictions over 5 repeats, with shaded areas indicating one standard deviation above and below the average. Dashed lines represent predictions of the eight-chain model.

at the percolation threshold is in good agreement with classical mean-field estimates: $\zeta_c \approx 0.6$ for diamond lattices [43], and $\zeta_c \approx 0.66$ for Bethe lattices [44]. Accelerated degradation kinetics in turn gives faster swelling (Fig. 5(b)) due the reduction in network elasticity, illustrated in Fig. 5(c), according to the Flory–Rehner condition (32). Fig. 5 also shows the predictions of the continuum model, where we assumed that $\eta = 1 - \zeta$. The performance of the continuum model is mainly limited by its ability to capture the elastic modulus, in particular near the percolation threshold. According to the EMA, the modulus tends to zero for $\zeta = 0.5$, which is significantly lower than the DN value (Fig. 5(c)). As a result, the continuum model overestimates the swelling ratio when ζ approaches the percolation threshold (Fig. 5(b)). The rate of chain scissions is however well predicted by the continuum model (Fig. 5(a)). It is in fact exact in the case $a = 0$ since the KMC algorithm is the discrete counterpart of the continuum kinetic model.

Interestingly, force-biased reaction ($a > 0$) leads to a larger reduction in the elastic modulus compared to the random chain scission case ($a = 0$) at the same degradation state ζ. This effect is shown in Fig. 6(a), where the evolution of degraded modulus is represented as a function of ζ. This directly contradicts the EMA (30), which assumes that the modulus reduction is one-to-one related to ζ. This additional kinetic effect on the modulus predicted by the DN model can be rationalised as follows. In random networks, the distribution of chain end-to-end distances and chain forces is heterogeneous. According to Eqs (20) and (22), the highly-stretched chains have a larger contribution to the elastic modulus. When $a > 0$, these highly-stretched chains are also more likely to be cut, therefore leading to a larger drop in modulus. This effect is illustrated in Fig. 6(b), which shows the probability distribution of chain end-to-end distance in undegraded ($\zeta = 0$) and degraded networks ($\zeta = 0.3$), for different values of a. As a increases, the distribution of chain end-to-end distances shifts to the left. Thus, force-biased degradation impacts the degradation pathway at the network level, which in turn leads to a reduced elastic modulus for the same number of chain scissions. This effect cannot be predicted by the continuum model, which assumes that all chains experience the same stretch and hence the same force. The effect of kinetics on network degradation is also apparent from the dependence of ζ_c on the activation length a. Close examination of Fig. 5 shows that ζ_c decreases

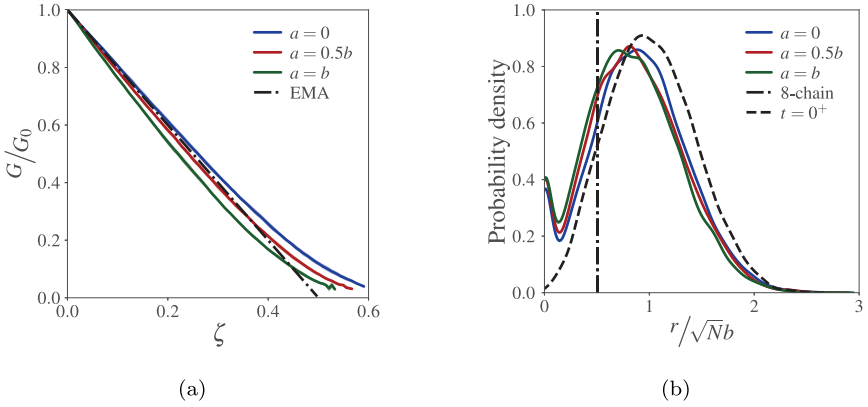

Fig. 6. (a) Normalised shear modulus as a function of the normalised number of chain scissions for different values of a. (b) Probability density of normalised chain end-to-end distance $\frac{r}{\sqrt{N}b}$ in undegraded ($\zeta = 0$) and degraded networks ($\zeta = 0.3$) for different values of activation length a. The chain end-to-end distance predicted using the eight-chain model is shown as a vertical dashed line.

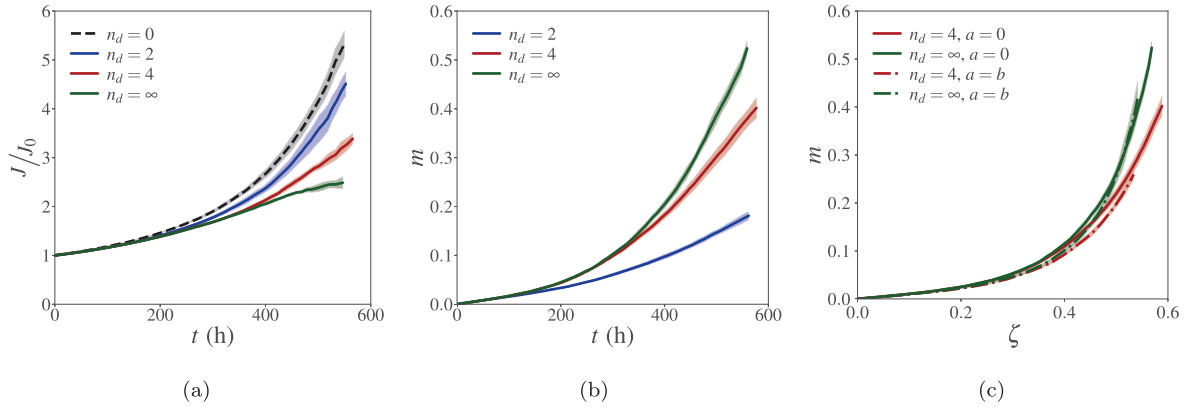

Fig. 7. DN predictions of (a) the normalised swelling ratio and (b) mass loss fraction as a function of time for different critical cluster sizes. The case $n_d = 0$ corresponds to no mass loss, whereas the case $n_d = \infty$ corresponds to the case where clusters of any size can diffuse. (c) DN predictions of the mass loss fraction for $a = 0$ and $a = b$ and two different critical cluster sizes. Lines represent the average DN predictions over 5 repeats, with shaded areas indicating one standard deviation above and below the average.

as a increases. This suggests that chains experiencing larger forces, and which are degraded preferentially when $a > 0$, are also more critical to the network connectivity. This phenomenon is closely related to the percolation of networks in which links are added or removed with a bias, which is a topic of current research [45,46].

We next examine the role of mass loss on degradation-induced swelling, as predicted by the DN model. Fig. 7 shows the evolution of (a) normalised swelling ratio J/J_0 and (b) mass loss fraction as a function of time for $a = 0$ and different critical cluster sizes n_d (similar trends are seen for $a > 0$). As expected, increasing n_d results in faster mass loss with no impact on the modulus (results not shown), since only elastically-ineffective clusters are removed. According to the Flory–Rehner condition (32), mass loss reduces the amount of swelling. Fig. 7(c) shows the mass loss fraction as a function of the normalised number of chain scissions ζ for two different critical cluster sizes and two values of the activation length. Results show that mass loss is largely independent of a for a given number of chain scissions ζ and given cluster size n_d. Note however that loss of percolation is reached at lower value of ζ in the case where $a > 0$, as previously observed in the case where $n_d = 0$.

4.2. Constrained degradation

Force-assisted degradation is expected to play a role in scenarios where degradation occurs under applied external forces. To illustrate this, we first consider degradation under a prescribed stretch, as illustrated in Fig. 3(b). At $t = 0^+$, the hydrogel is subjected to a uniaxial stretch λ_{1c} and let to swell freely in the two transverse directions to reach the equilibrium swelling ratio J_0. For $t > 0$, the hydrogel degrades while maintaining the applied stretch λ_{1c}. Details of the boundary conditions are given in Appendix A.2.

Fig. 8 shows the time evolution of (a) the normalised number of chain scissions ζ, (b) the swelling ratio J and (c) the nominal stress P_1 for three different values of the applied pre-stretch λ_{1c}, $a = b$ and no mass loss ($n_d = 0$). DN simulation results show an acceleration of the number of chain scissions with increasing pre-stretch, which directly follows from force-biased reaction kinetics (13). Like in the free-degradation case, DN results suggest that the percolation threshold ζ_c decreases with increasing pre-stretch. Accelerated degradation in turn leads to faster swelling and faster stress relaxation as λ_{1c} increases. In the case where $\lambda_{1c} = 1.1$, the evolution of P_1 is non-monotonic, which results from the competition between reduction in elasticity and swelling. The pre-stretch value $\lambda_{1c} = 1.1$ was selected so that is corresponds to the free swelling stretch, i.e. $P_1 = 0$ at $t = 0^+$. As the network starts to degrade under constant stretch λ_{1c}, a compressive state of stress develops since further swelling of the gel is hindered by the applied stretch. However, as degradation progresses, the elasticity of the gel reduces and the stress tends to zero. For $\lambda_{1c} = 2$ and $\lambda_{1c} = 3$, the applied pre-stretch is larger than the free-swelling stretch. Consequently, both degradation-induced swelling and elasticity reduction tend to decrease the stress, and P_1 monotonically relaxes to zero. Fig. 8 also shows the predictions of the continuum model. Overall, the continuum model is in good agreement with the DN model at early degradation stages, while deviations become more significant

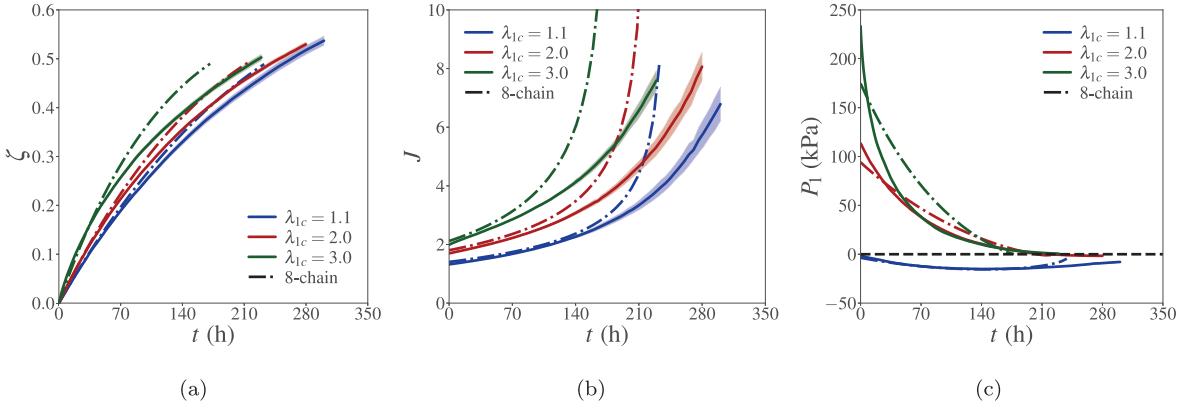

Fig. 8. (a) Normalised number of chain scissions, (b) swelling ratio, and (c) nominal stress P_1 as a function of time. Continuous lines represent the average DN predictions over 5 repeats, with shaded areas indicating one standard deviation above and below the average. Dashed lines represent predictions of the eight-chain model.

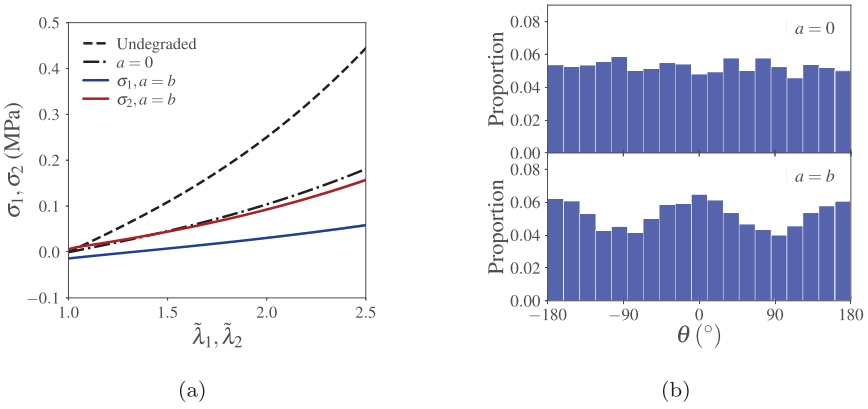

Fig. 9. (a) Stress–stretch curves of a network previously degraded for 80 h under a constant stretch $\lambda_{1c} = 3$. for $a = b$ and $a = 0$. Stretches $\tilde{\lambda}_i$ are measured relative to the degraded reference configuration. The responses of the undegraded network and that of a network with $a = 0$ and degraded up to the same value of ζ are also shown for comparison. (b) In a spherical coordinate system, the orientation of a chain in the reference configuration can be described by the polar and azimuthal angles (φ, θ). The distribution of θ for the broken chains for $\zeta = 0.3$ and $a = b$ shows that chains aligned with the loading direction ($\theta = 0° \pm 180°$) are preferentially broken, whereas the distribution is uniform for $a = 0$.

at advanced degradation stages. We conducted the same numerical experiments in the presence of mass loss. Similar to the free degradation case, mass loss does not impact the stress, but hinders swelling (results not shown for brevity). We also found that the activation length no significant impact on mass loss.

Force-biased degradation introduces anisotropy in the elastic properties. Fig. 9(a) shows the uniaxial stress–stretch response of networks previously subjected to constrained degradation with $\lambda_{1c} = 3$ for 80 h, corresponding to $\zeta = 0.3$. Uniaxial tension tests in direction 1 and 2 were performed w.r.t. to the degraded reference configuration. As expected, we observe anisotropy in the elastic response of degraded networks under force-accelerated kinetics in networks with $a = b$, with a softer response in direction 1 compared to direction 2. The figure also shows the response of the undegraded network, as well as that of a network with $a = 0$ and the same extent of degradation, $\zeta = 0.3$, which remains isotropic. The origin of anisotropic behaviour in the case $a = b$ is due to the preferential cutting of chains initially aligned in direction 1, whereas random cutting occurs in the case $a = 0$, see Fig. 9(b). In experiments, anisotropic behaviour of the degraded network could be used to probe whether force-assisted degradation occurs or not.

Finally, we consider degradation of a network under a dead load, as illustrated in Fig. 3(c). At $t = 0^+$, the hydrogel is subjected to a constant nominal stress P_0 in direction 1 and let to swell under zero stress in the other two directions. For $t > 0$, the hydrogel degrades under the constant dead load, see Appendix A.3 for details of boundary conditions. Fig. 10 shows (a) the normalised number of chain scissions, (b) the swelling ratio J and (c) the stretch λ_1 as a function of time in the case where $a = b$ and different values of the dead load P_0. Mass loss is neglected for simplicity ($n_d = 0$). Note that we used relatively small dead loads, because larger dead load values led to convergence issues in the numerical model. As a result, results in Fig. 10(a) show only a slight acceleration in the number of scission events as P_0 increases. However, the results indicate a decrease in the percolation threshold ζ_c with increasing loads, consistent with the previous degradation scenarios analysed. Despite the moderate acceleration in the number of scission events, the swelling ratio J and the stretch λ_1 evolve more rapidly with increasing dead load. Highly-stretched chains contributing the most to the network stiffness are more likely to break when $a > 0$, which in turn impacts the values of λ_1 and J. Predictions of the continuum model are also shown in Fig. 10. Like in the previous degradation cases, the continuum model has a good initial agreement with DN results, which is progressively lost as the percolation threshold is approached.

5. Conclusions

Force-biased degradation in rubbery networks was simulated in discrete networks using a Kinetic Monte Carlo (KMC) algorithm. By explicitly describing the evolving network structure, discrete networks naturally account for heterogeneous force distribution among the chains, which is turn impacts the local kinetics of chain scission. The discrete network model was also used to simulate mass loss following detachment of chain clusters from the main network. While this work focused on monodisperse network for simplicity, the computational model could be readily extended to polydisperse networks [15] or

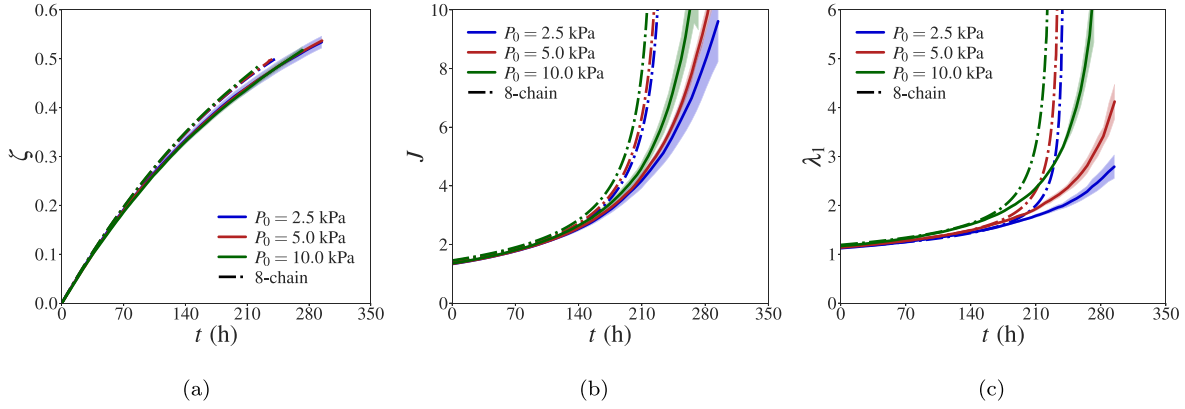

Fig. 10. (a) Normalised number of chain scissions, (b) swelling ratio, and (c) stretch as a function of time. Continuous lines represent the average DN predictions over 5 repeats, with shaded areas indicating one standard deviation above and below the average. Dashed lines represent predictions of the eight-chain model.

double networks [23]. The KMC algorithm could also be generalised to account for multiple reactive bonds along each chain, or for bonds with different reaction rate constants [21].

We have used the computational model to investigate the effect of force bias on free and constrained degradation. Key findings of this study are the following:

1. Force-biased reaction kinetics ($a > 0$) leads to a faster reduction in elastic modulus compared to the random case ($a = 0$), which in turn leads to faster swelling.
2. Furthermore, for a given degradation stage (i.e. a given number of chain scissions), the reduction in modulus is more significant in the case of force-biased degradation, because chains bearing larger loads are cut preferentially. Loss of percolation also requires a smaller number of chain scission events with force-biased degradation.
3. Force-biased reaction kinetics induces damage anisotropy when degradation occurs under external loads. We propose that anisotropy in the elastic properties after degradation under loads could be used to experimentally verify whether reaction kinetics is biased by forces or not.

We also developed a simple micromechanics-based continuum model, building on the widely used 8-chain representation [16] combined with a rate-dependent chain scission model following Lavoie et al. [40]. The effect of damage by chain scission on the modulus was captured using an Effective Medium Approximation [41], which holds at early degradation stages [19], but fails to capture reverse gelation. This limitation of the EMA was identified in our previous work [32]. Advanced models are needed to describe the reduction in modulus with degradation up to the point of reverse gelation, and ideally such models should be micromechanics-based. Better predictions have been obtained based on tree-like theory [32,39], however the micromechanics-basis of these approaches is unclear and therefore they remain largely phenomenological. Another intrinsic limitation of a continuum model based on the eight-chain representation is that it does not account for the heterogeneous chain force distribution. To address this issue, a model that explicitly accounts for the distribution of chain stretches and its evolution during degradation should be adopted, and non-affine localisation rules for the chain stretch should be considered, see e.g. Araujo et al. [15],Vernerey et al. [47],Diani and Le Tallec [48],Mulderrig et al. [49]. The model should also be able to describe anisotropic damage.

CRediT authorship contribution statement

Lucas Mangas Araujo: Writing – original draft, Validation, Software, Methodology, Investigation, Formal analysis, Conceptualization.

Laurence Brassart: Writing – review & editing, Supervision, Methodology, Investigation, Funding acquisition, Formal analysis, Conceptualization.

Declaration of competing interest

The authors declare that they have no known competing financial interests or personal relationships that could have appeared to influence the work reported in this paper.

Acknowledgements

The authors would like to thank Dr Ivan Kryven (University of Utrecht) for insightful discussions. L.B. acknowledges the support of a Future Leaders Fellowship of UK Research and Innovation [MR/W006995/1]. L.M.A. is supported by The Clarendon Fund in partnership with the Jesus College Old Members Scholarship, and by The Jesus College Graduate Scholarship.

Appendix A. Details of boundary conditions

A.1. Free degradation

Degradation-induced swelling of a network under no external loads is illustrated in Fig. 3(a). The deformation gradient is of the form $\boldsymbol{F} = \lambda_s \mathbf{1}$, where λ_s is the swelling stretch, and $J = \lambda_s^3$. At time $t = 0^+$, the undegraded network is immersed in a water bath with $\mu = \mu_0$ and instantaneously swells to its equilibrium value, $J = J_0$. As the network degrades ($t > 0$), its elastic modulus decreases and the equilibrium swelling ratio increases. Affine boundary conditions corresponding to the current swelling stretch are applied according to Eq. (10). For isotropic, free swelling, $\boldsymbol{\sigma} = \mathbf{0}$ and the network stress is of the form $\boldsymbol{\sigma}^e = \sigma^e \mathbf{1}$. The state law (8) identifies the Lagrange multiplier as $\Pi = \sigma^e = \frac{1}{\lambda_s^2}\frac{\partial \psi^e}{\partial \lambda_s}$, which can be calculated for a given value of λ_s from the reaction forces on the DN according to Eq. (11). The state law (12) provides:

$$0 = k_B T \left[\log(1-\phi) + \phi + \chi\phi^2\right] + \Omega\sigma^e, \tag{32}$$

where we recall that $(1-\phi) = \Omega C/J$ and $J = \lambda_s^3$ is related to water concentration (and mass loss fraction) by the incompressibility condition (6). At each time step, Eq. (32) is solved iteratively for λ_s using the `scipy.optimize` library in Python, adjusting the affine boundary conditions (10). Eq. (32) is equivalent to the Flory–Rehner model [50], according to which equilibrium swelling follows from the balance of elastic and mixing energies. Simulations are interrupted when the percolation criterion is met, corresponding to a critical number of chain scissions ζ_c.

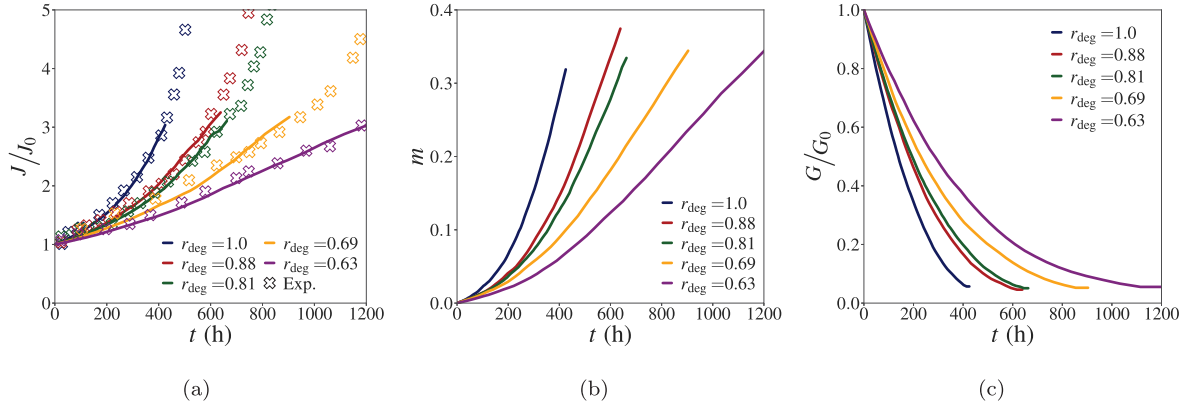

Fig. 11. Degradation behaviour of tetra-PEG hydrogels with different fractions of degradable chains r_{deg}: (a) normalised swelling ratio, (b) mass loss fraction, and (c) normalised degraded shear modulus. Continuous lines represent the average response of five DN simulations, and symbols are experimental data taken from Li et al. [39].

A.2. Degradation under a constant stretch

Degradation of a network subjected to a constant stretch is illustrated in Fig. 3(b). At $t = 0^+$, the network is subjected to a uniaxial stretch λ_{1c} and let to swell freely in the two transverse directions: $\sigma_2 = \sigma_3 = 0$ to reach the equilibrium swelling ratio J_0. For $t > 0$, the network degrades while maintaining the applied stretch λ_{1c}. The Lagrange multiplier during degradation is obtained from Eq. (8): $\sigma_2^e = \Pi$, and the stretches in the transverse directions $\lambda_2 = \lambda_3$ are obtained from the state law (12):

$$0 = k_B T \left[\log(1-\phi) + \phi + \chi\phi^2\right] + \Omega\sigma_2^e. \tag{33}$$

Similar to the free swelling case, Eq. (33) is solved iteratively for the transverse stretches. The true stress in the direction of the applied stretch is given by $\sigma_1 = \sigma_1^e - \Pi = \sigma_1^e - \sigma_2^e$, and the corresponding nominal stress is calculated as:

$$P_1 = \lambda_2^2 \left(\sigma_1^e - \sigma_2^e\right). \tag{34}$$

A.3. Swelling under a dead load

Degradation-induced swelling of a hydrogel under a dead load is illustrated in Fig. 3(c). At $t = 0^+$, the network is subjected to a constant nominal stress P_0 in direction 1 and let to swell under zero stress in other two directions: $\sigma_2 = \sigma_3 = 0$. For $t > 0$, the network degrades under the constant dead load. The equilibrium state of the gel is found by solving the following system of equations:

$$P_0 = \frac{J}{\lambda_1}\left(\sigma_1^e - \Pi\right), \tag{35}$$

$$0 = \sigma_2^e - \Pi, \tag{36}$$

$$0 = k_B T \left[\ln(1-\phi) + \phi + \chi\phi^2\right] + \Omega\Pi, \tag{37}$$

for the three unknowns λ_1, λ_2 and Π.

Appendix B. Application to tetra-PEG hydrogels

To illustrate the DN modelling framework capability using realistic parameters, we compare its predictions to experimental data for tetra-PEG hydrogels with tunable degradability developed by [39]. These gels were formed by the crosslinking in solution of four-arm PEG macromolecules with well-defined arm length, leading to near-ideal network structures [51]. Degradability of the hydrogel was achieved by functionalising a given fraction of the tetra-arm precursors with degradable ester bonds. The ester bonds can react with water molecules, causing hydrolytic chain scission. In the experiments, as-prepared hydrogels with different fractions r_{deg} of degradable chains were immersed in a water bath, and let to swell freely as hydrolytic degradation proceeds, and the swelling ratio as a function of time was recorded.

Material parameters used in the DN model were directly obtained from experimental testing conditions whenever possible. The molecular weight of the four-arm precursors was $M_w = 10$ kDa in the experiments, giving $n_m = \frac{M_w}{2M_1} = 113$ PEG monomers per chain (a chain consists of two arms of the four-arm macromolecule precursor), with $M_1 = 44$ g/mol the molar mass of one PEG molecule. The contour length of each chain was estimated as $L_c = n_m l_p$, where $l_p = 0.28$ nm is the projected monomer length in the trans-trans-gauche configuration [52]. The Kuhn length of PEG was set to $b = 1.1$ nm [53], giving the number of Kuhn segments as $N = L_c/b = 29$. The volume per water molecule was set to $\Omega = 3 \times 10^{-29}$ m^3, the temperature was set to $T = 310$ K and the Flory–Huggins interaction parameter was set to $\chi = 0.45$ [39]. To simplify parameter identification, we neglected the effect of force-assisted degradation and set $a = 0$. In fact, it is unclear from the literature whether hydrolytic degradation of ester bonds is activated by force or not [54–56]. Answering this question is outside the scope of this paper. In the DN simulations, the only fitting parameters were the reaction rate constant k_0 and the critical cluster size for mass loss, n_d.

Perfect random networks were generated with chain density given by:

$$\nu^* = \frac{2\phi_0 \rho N_a}{M_w}, \tag{38}$$

where $\rho = 1.12$ g/cm^3 is the density of PEG, $\phi_0 = 0.053$ is the volume fraction of polymer [39], and N_a is the Avogadro number. The average end-to-end distance between crosslinks in the random network was set to the corresponding distance in a diamond lattice at the same density ν^*, $\langle r_0 \rangle \approx \frac{\sqrt{3}}{4^{1/3}}(\nu^*)^{-1/3}$ [57] using our network generation algorithm allowing independent control of chain density and average chain end-to-end distance [15]. Next, connectivity defects were introduced by randomly cutting a fraction $(1 - p_0)$ of the chains, with $p_0 = 0.86$ [39], creating dangling ends. Finally, a fraction r_{deg} of the chains was flagged as degradable. In the equilibrated reference configuration, the average end-to-end distance of the chains was $\langle r_0 \rangle \approx 0.96\sqrt{N}b$.

Degradation-induced swelling was simulated by instantaneously swelling the undegraded network to its equilibrium value under chemical potential $\mu = \mu_0$ at time $t = 0^+$, and then letting the network degrade and swell further for $t > 0$, see Fig. 3(a). Fig. 11(a) shows the normalised swelling ratio $\frac{J}{J_0}$ predicted by the model for tetra-PEG gels with varying fractions of degradable chains r_{deg}, where J_0 is the equilibrium swelling ratio at $t = 0^+$. The reaction constants, fitted for each curve, are listed in Table 1, and we set $n_d = 4$ in all simulations. The model generally produces satisfactory predictions at all values of r_{deg}, and the fitted k_0 are all relatively close, consistent with a single

Table 1
Fitted values of the reaction constant k_0 for different fractions of degradable chains r_{deg}. The average reaction constant over all r_{deg} is $k_0 = 15.1 \times 10^{-4}$ h^{-1}.

Fraction of degradable chains r_{deg}	Reaction constant k_0 (h^{-1})
1.0	16.5×10^{-4}
0.88	14.5×10^{-4}
0.81	15.0×10^{-4}
0.69	15.5×10^{-4}
0.63	14.0×10^{-4}

reaction mechanism. Simulations were interrupted upon reaching the percolation transition, which occurred before the experimental final degradation time. However, simulations stopped close to the point where the experimental curve sharply increases, which is an indication of reverse gelation in the experiments. Figs. 11(b) and (c) respectively show the predicted evolution of the mass loss m and normalised shear modulus $\frac{G}{G_0}$ (experimental data were not reported for these quantities). Overall, model predictions appear reasonable, indicating that gels with a lower fraction of degradable chains display slower mass loss and modulus reduction.

Data availability

Data will be made available on request.

References

[1] S. Lyu, D. Untereker, Degradability of polymers for implantable biomedical devices, Int. J. Mol. Sci. 10 (9) (2009) 4033–4065.
[2] K. Bensalem, M. Eesaee, M. Hassanipour, S. Elkoun, E. David, K. Agbossou, P. Nguyen-Tri, Lifetime estimation models and degradation mechanisms of elastomeric materials: a critical review, Polym. Degrad. Stab. (2023) 110644.
[3] J. Ribas-Arino, D. Marx, Covalent mechanochemistry: theoretical concepts and computational tools with applications to molecular nanomechanics, Chem. Rev. 112 (10) (2012) 5412–5487.
[4] S. Zhurkov, V. Korsukov, Atomic mechanism of fracture of solid polymers, J. Polym. Sci.: Polym. Phys. Ed. 12 (2) (1974) 385–398.
[5] V. Bershtein, L. Egorova, V. Solov'ev, Disintegration of polymers by a hydrolytic mechanism, Polym. Mech. 13 (5) (1977) 715–721.
[6] X. Yang, J. Yang, L. Chen, Z. Suo, Hydrolytic crack in a rubbery network, Extrem. Mech. Lett. 31 (2019) 100531.
[7] N. Qari, S. Cai, Stress-assisted erosion of poly (glycerol-co-sebacate) acrylate elastomer, Macromol. Chem. Phys. 225 (4) (2024) 2300268.
[8] E.M. Lloyd, J.R. Vakil, Y. Yao, N.R. Sottos, S.L. Craig, Covalent mechanochemistry and contemporary polymer network chemistry: A marriage in the making, J. Am. Chem. Soc. 145 (2) (2023) 751–768.
[9] S. Aydonat, A.H. Hergesell, C.L. Seitzinger, R. Lennarz, G. Chang, C. Sievers, J. Meisner, I. Vollmer, R. Göstl, Leveraging mechanochemistry for sustainable polymer degradation, Polym. J. 56 (4) (2024) 249–268.
[10] Z.J. Wang, J.P. Gong, Mechanochemistry for on-demand polymer network materials, Macromolecules 58 (1) (2025) 4–17.
[11] K. Kothari, Y. Hu, S. Gupta, A. Elbanna, Mechanical response of two-dimensional polymer networks: Role of topology, rate dependence, and damage accumulation, J. Appl. Mech. 85 (3) (2018) 031008.
[12] G. Alamé, L. Brassart, Relative contributions of chain density and topology to the elasticity of two-dimensional polymer networks, Soft Matter 15 (28) (2019) 5703–5713.
[13] J. Lei, Z. Liu, A network mechanics method to study the mechanism of the large-deformation fracture of elastomers, J. Appl. Phys. 132 (13) (2022).
[14] R.J. Wagner, J. Dai, X. Su, F.J. Vernerey, A mesoscale model for the micromechanical study of gels, J. Mech. Phys. Solids 167 (2022) 104982.
[15] L.M. Araujo, I. Kryven, L. Brassart, Micromechanical modelling of rubbery networks: The role of chain pre-stretch, Int. J. Non-Linear Mech. 166 (2024) 104834.
[16] E.M. Arruda, M.C. Boyce, A three-dimensional constitutive model for the large stretch behavior of rubber elastic materials, J. Mech. Phys. Solids 41 (2) (1993) 389–412.
[17] P. Wu, E. Van Der Giessen, On improved network models for rubber elasticity and their applications to orientation hardening in glassy polymers, J. Mech. Phys. Solids 41 (3) (1993) 427–456.
[18] A.A. Gusev, Numerical estimates of the topological effects in the elasticity of gaussian polymer networks and their exact theoretical description, Macromolecules 52 (9) (2019) 3244–3251.
[19] G. Alamé, L. Brassart, Effect of topological defects on the elasticity of near-ideal polymer networks, J. Appl. Mech. 87 (12) (2020) 121006.
[20] A. Arora, T.-S. Lin, B.D. Olsen, Coarse-grained simulations for fracture of polymer networks: Stress versus topological inhomogeneities, Macromolecules 55 (1) (2022) 4–14.
[21] H.K. Beech, S. Wang, D. Sen, D. Rota, T.B. Kouznetsova, A. Arora, M. Rubinstein, S.L. Craig, B.D. Olsen, Reactivity-guided depercolation processes determine fracture behavior in end-linked polymer networks, ACS Macro Lett. 12 (12) (2023) 1685–1691.
[22] B. Deng, S. Wang, C. Hartquist, X. Zhao, Nonlocal intrinsic fracture energy of polymerlike networks, Phys. Rev. Lett. 131 (22) (2023) 228102.
[23] H. Li, J. Lei, D. Wang, Z. Liu, The fracture and toughening mechanism of double-network hydrogel using the network mechanics method, Eng. Fract. Mech. 309 (2024) 110413.
[24] S.J. Bryant, F.J. Vernerey, Programmable hydrogels for cell encapsulation and neo-tissue growth to enable personalized tissue engineering, Adv. Heal. Mater. 7 (1) (2018) 1700605.
[25] B. Turner, S. Ramesh, S. Menegatti, M. Daniele, Resorbable elastomers for implantable medical devices: highlights and applications, Polym. Int. 71 (5) (2022) 552–561.
[26] B. Hosseinzadeh, M. Ahmadi, Degradable hydrogels: Design mechanisms and versatile applications, Mater. Today Sustain. 23 (2023) 100468.
[27] C.K. Lee, C.E. Diesendruck, E. Lu, A.N. Pickett, P.A. May, J.S. Moore, P.V. Braun, Solvent swelling activation of a mechanophore in a polymer network, Macromolecules 47 (8) (2014) 2690–2694.
[28] D.W. Kim, G.A. Medvedev, J.M. Caruthers, J.Y. Jo, Y.-Y. Won, J. Kim, Enhancement of mechano-sensitivity for spiropyran-linked poly (dimethylsiloxane) via solvent swelling, Macromolecules 53 (18) (2020) 7954–7961.
[29] F.K. Metze, S. Sant, Z. Meng, H.-A. Klok, K. Kaur, Swelling-activated, soft mechanochemistry in polymer materials, Langmuir 39 (10) (2023) 3546–3557.
[30] P.J. Flory, Thermodynamics of high polymer solutions, J. Chem. Phys. 10 (1) (1942) 51–61.
[31] M.L. Huggins, Some properties of solutions of long-chain compounds, J. Phys. Chem. 46 (1) (1942) 151–158.
[32] Z. Pan, L. Brassart, Constitutive modelling of hydrolytic degradation in hydrogels, J. Mech. Phys. Solids 167 (2022) 105016.
[33] W. Kauzmann, H. Eyring, The viscous flow of large molecules, J. Am. Chem. Soc. 62 (11) (1940) 3113–3125.
[34] G.I. Bell, Models for the specific adhesion of cells to cells: a theoretical framework for adhesion mediated by reversible bonds between cell surface molecules, Science 200 (4342) (1978) 618–627.
[35] Y. Mao, B. Talamini, L. Anand, Rupture of polymers by chain scission, Extrem. Mech. Lett. 13 (2017) 17–24.
[36] J. Zhu, L. Brassart, Stretching response of a polymer chain with deformable bonds, 2025, arXiv:2502.08602, URL https://arxiv.org/abs/2502.08602.
[37] A.F. Voter, Introduction to the kinetic Monte Carlo method, in: Radiation Effects in Solids, Springer, 2007, pp. 1–23.
[38] A.P. Thompson, H.M. Aktulga, R. Berger, D.S. Bolintineanu, W.M. Brown, P.S. Crozier, P.J. In't Veld, A. Kohlmeyer, S.G. Moore, T.D. Nguyen, et al., LAMMPS-a flexible simulation tool for particle-based materials modeling at the atomic, meso, and continuum scales, Comput. Phys. Comm. 271 (2022) 108171.
[39] X. Li, Y. Tsutsui, T. Matsunaga, M. Shibayama, U.-i. Chung, T. Sakai, Precise control and prediction of hydrogel degradation behavior, Macromolecules 44 (9) (2011) 3567–3571.
[40] S.R. Lavoie, R. Long, T. Tang, A rate-dependent damage model for elastomers at large strain, Extrem. Mech. Lett. 8 (2016) 114–124.
[41] K. Nishi, M. Chijiishi, Y. Katsumoto, T. Nakao, K. Fujii, U.-i. Chung, H. Noguchi, T. Sakai, M. Shibayama, Rubber elasticity for incomplete polymer networks, J. Chem. Phys. 137 (22) (2012).
[42] K. Nishi, K. Fujii, U.-i. Chung, M. Shibayama, T. Sakai, Experimental observation of two features unexpected from the classical theories of rubber elasticity, Phys. Rev. Lett. 119 (26) (2017) 267801.
[43] D. Stauffer, A. Aharony, Introduction to Percolation Theory, Taylor & Francis, 2018.
[44] M. Rubinstein, R.H. Colby, Polymer Physics, Oxford University Press, 2003.
[45] J. Spencer, N. Wormald, Birth control for giants, Combinatorica 27 (2007) 587–628.
[46] D. Achlioptas, R.M. D'souza, J. Spencer, Explosive percolation in random networks, Science 323 (5920) (2009) 1453–1455.
[47] F.J. Vernerey, R. Brighenti, R. Long, T. Shen, Statistical damage mechanics of polymer networks, Macromolecules 51 (17) (2018) 6609–6622.
[48] J. Diani, P. Le Tallec, A fully equilibrated microsphere model with damage for rubberlike materials, J. Mech. Phys. Solids 124 (2019) 702–713.
[49] J. Mulderrig, B. Li, N. Bouklas, Affine and non-affine microsphere models for chain scission in polydisperse elastomer networks, Mech. Mater. 160 (2021) 103857.

[50] P.J. Flory, J. Rehner, Statistical mechanics of cross-linked polymer networks. II. Swelling, J. Chem. Phys. 11 (11) (1943) 521–526.
[51] T. Sakai, T. Matsunaga, Y. Yamamoto, C. Ito, R. Yoshida, S. Suzuki, N. Sasaki, M. Shibayama, U.-i. Chung, Design and fabrication of a high-strength hydrogel with ideally homogeneous network structure from tetrahedron-like macromonomers, Macromolecules 41 (14) (2008) 5379–5384.
[52] F. Oesterhelt, M. Rief, H. Gaub, Single molecule force spectroscopy by AFM indicates helical structure of poly (ethylene-glycol) in water, New J. Phys. 1 (1) (1999) 6.
[53] A. Dittmore, D.B. McIntosh, S. Halliday, O.A. Saleh, Single-molecule elasticity measurements of the onset of excluded volume in poly (ethylene glycol), Phys. Rev. Lett. 107 (14) (2011) 148301.
[54] S. Akbulatov, Y. Tian, E. Kapustin, R. Boulatov, Model studies of the kinetics of ester hydrolysis under stretching force, Angew. Chem. 125 (27) (2013).
[55] J. Wang, X. Gao, A. Boarino, F. Célerse, C. Corminboeuf, H.-A. Klok, Mechanical acceleration of ester bond hydrolysis in polymers, Macromolecules 55 (22) (2022) 10145–10152.
[56] H. Lei, Q. Ma, Z. Wang, D. Zhang, X. Huang, M. Qin, H. Ma, W. Wang, Y. Cao, Ester bond: chemically labile yet mechanically stable, ACS Nano 17 (17) (2023) 16870–16878.
[57] T. Matsunaga, T. Sakai, Y. Akagi, U.-i. Chung, M. Shibayama, SANS and SLS studies on tetra-arm PEG gels in as-prepared and swollen states, Macromolecules 42 (16) (2009) 6245–6252.